REPORT DOCUMENTATION PAGE

Form Approved
OMB No. 0704-0188

1. AGENCY USE ONLY (Leave Blank)	2. REPORT DATE 21 April 2004	3. REPORT TYPE AND DATES COVERED Final Report, 19 Feb 92 - 31 Dec 03

4. TITLE AND SUBTITLE
Final Technical Report

5. FUNDING NUMBERS
N00014-01-G-0460
Task Order 0003

6. AUTHOR(S)
Marilee Andrew, Shahram Vaezy, Peter Kaczkowski, Steven Kargl, Daniel Rouseff,
Kirk Beach, Siddhartha Sikdar, R. Lee Thompson, and Lawrence Crum

7. PERFORMING ORGANIZATION NAME(S) AND ADDRESS(ES)
Applied Physics Laboratory, University of Washington
Box 355640, 1013 NE 40th St.
Seattle WA 98105-6698

8. PERFORMING ORGANIZATION REPORT NUMBER
N/A

9. SPONSORING/MONITORING AGENCY NAME(S) AND ADDRESS(ES)
Office of Naval Research, Code 341
800 N Quincy St. Room 823-6
Arlington VA 22217-5660

10. SPONSORING/MONITORING AGENCY REPORT NUMBER

11. SUPPLIMENTARY NOTES

12a. DISTRIBUTION/AVAILABILITY STATEMENT
Unlimited

12b. DISTRIBUTION CODE

13. ABSTRACT (Maximum 200 words)

This report summarizes research efforts conducted under the ONR grant entitled "An Acoustic Hemostasis Device for Acute Arterial Bleeding, " Lawrence Crum, Principal Investigator. The revised scope of effort concentrated on four tasks: Bleeding Detection, Therapy Delivery, Systems Design and Development, and Animal Testing of Systems. The revised performance period was 19 February 2002 - 31 December 2003.

BEST AVAILABLE COPY

20040427 158

14. SUBJECT TERMS
Hemhorrage control, hemostasis, focused ultrasound

15. NUMBER OF PAGES
28

16. PRICE CODE

17. SECURITY CLASSIFICATION OF REPORT Unclassified	18. SECURITY CLASSIFICATION OF THIS PAGE Unclassified	19. SECURITY CLASSIFICATION OF ABSTRACT Unclassified	20. LIMITATION OF ABSTRACT Unlimited

DISTRIBUTION STATEMENT A
Approved for Public Release
Distribution Unlimited

FINAL TECHNICAL REPORT
ONR ORDER NUMBER N00014-01-G-0460 0003
"AN ACOUSTIC HEMOSTASIS DEVICE FOR ACUTE
ARTERIAL BLEEDING"
Lawrence A. Crum, Principal Investigator

I.   INTRODUCTION

The original objective of this research was to construct a lightweight, portable, transcutaneous acoustic hemostasis system using Doppler targeting to locate a jet of blood exiting from an injured artery. The research plan anticipated integrating into this system an annular HIFU array capable of delivering the necessary acoustic energy to induce hemostasis within a range of vessel depths. The original performance period was 19 February 2002 – 18 February 2005. Program funding was cut back, however, from $2,994,875 to $1,580,000, and the performance period was revised to 19 February 2002 – 31 December 2003. As a result of these program cuts, research efforts were scaled back and the work integrated with research efforts funded by the U.S. Army. This final report summarizes the accomplishments achieved within the revised level of effort and funding.

The specific aims of the original grant included:

1. To investigate various techniques and methods to detect and localize acute arterial bleeding.
2. To investigate various techniques and methods to induce acoustic hemostasis in acute arterial bleeds through the optimal delivery of HIFU energy.
3a. To develop an image-guided, HIFU test-bed to examine the optimal conditions for the transcutaneous treatment of near surface arterial bleeds.
3b. To develop a Doppler-guided, HIFU test-bed to examine the optimal conditions for the transcutaneous treatment of near surface arterial bleeds.
4. To optimize, test, and demonstrate these units in animal models.
5. To utilize the results of (1) though (4) to design an engineering prototype suitable for human clinical tests.

Table 1 presents the original Gantt chart of individual project tasks. The reduced scope of effort focused on the following areas within those original project tasks:

Task 1.00 Bleeding Detection: Implementation of vibrometry algorithms on a commercial imaging machine (Subtask 1.20). Accomplishments are discussed in Section II.A of this report.

Task 2.00 Therapy Delivery: (a) development of real-time HIFU lesion imaging using RF backscatter monitoring techniques (Task 2.10) and (b) development of bioacoustic models and associated *in vitro studies* (Subtask 2.20). Accomplishments are discussed in Section II.B of this report.

Task 3.00 Systems Design and Development: (a) novel transducer development (Subtask 3.20), (b) improvements to the Sonics concepts phased array and associated drive electronics (Subtasks 3.20 and 3.31), and (c) initial assembly and testing of the Imasonic array (Subtasks 3.20 and 3.31). Accomplishments are discussed in Section II.C of this report.

Task 4.00 Animal testing of systems: Image-Guided Animal Tests Unit 1 (Subtask 4.10). Accomplishments are discussed in Section II.D of this report.

Figure 1. Gantt Chart of Original Proposal

#	TASK DESCRIPTION / FY	2002	2003	2004	2005
1.00	**Bleeding Detection**				
1.10	Bleeding Patterns - Animal Studies		▒		
1.20	Ultrasonic Vibrometer		▒		
1.30	Doppler Detection and Localization			▒	
2.00	**Therapy Delivery**				
2.10	HIFU Lesion Imaging	∿∿∿∿∿∿∿∿∿∿∿			
2.20	Modeling	∿∿∿∿∿∿∿∿∿∿∿			
3.00	**Systems Design and Development**				
3.10	Requirements and Planning		▤	▤	
3.20	Transducer Development				
3.21	Aperture and Focusing Design		▓▓▓▓		
3.22	Array Design		▓▓▓▓		
3.23	Fabrication/Testing of Integrated Assemblies		▓▓▓▓▓▓▓		
3.30	Electronic System Development				
3.31	Image-Guided System: Test Unit 1	▥▥▥▥▥			
3.32	System Upgrades to Test Unit 1			▥▥▥▥	
3.33	Doppler-Guided System: Test Unit 2		▥▥▥		
4.00	**Animal Testing of Systems**				
4.10	Image-Guided Animal Tests Unit 1		☒☒☒☒☒		
4.20	Doppler-Guided Animal Tests, Unit 2			☒	
5.00	**Clinical Unit Design**				▣

Key accomplishments of the research included:

- Vibrometry bleeding detection algorithms have been implemented on a commercial imaging machine, and initial *in vivo* testing was completed.
- Algorithms for collecting, processing, and interpreting RF ultrasound imaging data to infer local temperature rise have been developed. A pilot study using thermocouple instrumented gel phantoms and both HIFU and hot wire sources has been performed. Results indicate promise for the method.
- A pilot study using linear and circular scanning HIFU protocols was performed to investigate novel treatment protocols, investigate the effects of nonlinear acoustics, and validate numerical models.

- Numerical models including Khohklov-Zabolotskaya-Kuznetsov (KZK) and Parabolic Equation (PE) implementations to simulate the HIFU acoustic field, coupled with the BioHeat Transfer Equation (BHTE) to simulate the temperature field.
- Two HIFU arrays, one built by Sonic Concepts, Inc. and one built by Imasonic, were constructed during the reporting period. Driving electronics built principally by Sonic Concepts, Inc. were modified for use with the Sonic Concepts probe; the Imasonic array interfaces with a drive system manufactured by Advanced Surgical Systems, Inc..
- An *in vivo* study was completed investigating the optimal parameters, including acoustic intensity, tissue temperature and treatment time, for inducing acoustic hemostasis. A further *in vivo* study was performed to investigate the utility of tissue homogenate formation in decreasing hemostasis time.

The following sections summarize work accomplished under this grant. Detailed discussion of the research may be found in the papers, sponsored partially or fully by support from this grant, listed in Section V. Publications, and also in the 2002 and 2003 ONR Annual Reports submitted to the project office. A selection of reprints from the Publications list is provided in the Appendix and includes a copy of a conference proceedings volume sponsored in part by ONR.

II. RESEARCH ACCOMPLISHMENTS

II.A. Bleeding Detection and Localization (Subtask 1.20)

II.A.1 Implementation of vibrometry on a commercial imaging machine

Arterial bleeding into a free space is known to cause local vibrations in tissue. Under this grant we developed an algorithm for detection of small amplitude vibrations using ensemble data acquired using a color-flow ultrasound system. Using this algorithm, two dimensional images of the vibration amplitude, frequency and phase can be created, and these two-dimensional images may be used for localizing the source of vibrations caused by internal bleeding. This algorithm has been implemented in a programmable ultrasound system to study the usefulness of tissue vibrations for real-time localization of bleeding sites in animals.

A vibrating target with amplitude a_0 and frequency f_{vib} modulates the phase of the mth received ultrasound echo, $y(\tau,m)$, according to the following equation.

$$y(\tau,m) = A(\tau)e^{j2\pi f_0(\frac{2a_0 \sin(2\pi m T_{PRF} f_{vib})}{c})}, \qquad (1)$$

where $A(\tau)$ is the complex amplitude of the scattered signal, f_0 is the center frequency of the transducer, T_{PRF} is the pulse repetition interval, and c is the speed of sound. Slow-moving tissue and blood flow affect the phase of $A(\tau)$. Conventional color-flow imaging systems utilize clutter filters for suppressing the effects of slow-moving tissue, and emphasizing the blood flow. Tissue vibrations that are not suppressed by these clutter filters are manifested as a characteristic checkered pattern in the color-flow image. Due to the small number of temporal samples, conventional filtering-based approaches lack sufficient resolution to separate the tissue vibrations from blood flow and other non-oscillatory tissue motion. Therefore, a new high-resolution

signal-processing algorithm is needed. We have utilized eigendecomposition-based techniques to isolate and characterize vibrations.

Prior to detecting vibrations using our algorithm, any constant-velocity motion components are removed from the received echo. The mean velocity of motion is estimated using autocorrelation, and subtracted using a clutter shift operation. The phase of the resulting signal is then computed. An approximate eigendecomposition using the QR factorization algorithm is then used for separating the phase into its dominant components. Echoes from moving tissue are expected to be more coherent than those from blood and random noise. Thus, most of the energy will be distributed in a small number of dominant components. High-frequency signals that have more than a certain fraction, T, of the total energy contained in the two dominant components are detected as potential vibrations. Optimum values for the threshold T can be determined through simulation. The mean amplitude and frequency of the vibrations are estimated from the Hilbert Transform of the phase signal by using the autocorrelation method.

We have implemented this algorithm on a programmable ultrasound system that uses a new generation of high-performance processors known as mediaprocessors to perform all back-end ultrasound signal-processing operations in software. Although our algorithm requires computationally prohibitive operations such as eigendecomposition, careful mapping of the algorithm to the underlying processor architecture has enabled us to achieve a processing throughput that closely matches the acquisition rate of a conventional ultrasound system.

The performance of our detection and estimation algorithm was evaluated using Monte Carlo simulation. The received echo was modeled using the parameters specified in Table 1 with randomly generated tissue and blood velocity. For each realization, three separate signals were generated: clutter-only, clutter with blood flow, and clutter with vibration but without blood flow. False positive cases were those where vibrations were detected in the blood or clutter signal while false negatives were those in which vibrations failed to be detected in the signal with vibration. The detector performance was evaluated with different threshold settings to measure the sensitivity and specificity.

Table 1. Simulation parameters for detector evaluation.

Clutter to blood signal ratio	Flow signal to noise ratio	Ensemble size	Pulse repetition frequency
40 dB	3-10 dB	16	400 Hz
Center frequency	Vibration amplitude	Vibration frequency	Number of realizations
3.5 MHz	10 mm	100 Hz	10,000

Figure 2 (a) and (b) shows the detection sensitivity and specificity of our algorithm. For thresholds less than 20, the sensitivity is greater than 96 %. An optimal threshold setting can be computed by selecting an operating point in the receiver operating characteristic (ROC) shown in Fig. 2 (c). According to Fig. 2 (c), it can be seen that a sensitivity of 96 % and a specificity of 99 % can be achieved even for SNR as low as 3 dB. The corresponding optimum threshold setting can then be found from Fig. 1 (a) or (b).
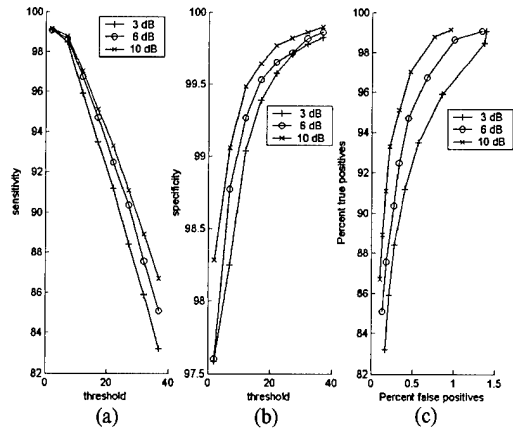
Figure 2. Detector evaluation.

Prior to using this algorithm for *in vivo* studies, we performed some phantom experiments for validation. A schematic of the experimental setup is shown in Fig. 3 (a). A piezoelectric vibrating disc immersed in a water bath was oscillated at a known frequency (500 Hz) using a function generator. This plate was then imaged using ultrasound, and the vibration amplitude image was generated by applying our algorithm to the color-flow ensemble data acquired from the ultrasound system. A 7.5-Mhz ultrasound probe with an ensemble length of 10 @ 2 kHz PRF was used. Figure 3 (b) shows the B-mode image of the plate overlaid with the vibration amplitude image. The vibration amplitude is maximum at the center of the disc and decreases towards the edges. This behavior is expected, since the disc is attached to the base at edges, thus the displacement at the edges is constrained to be zero.

We also performed experiments to determine the accuracy of the ultrasonically measured vibration parameters. The amplitude of the vibrating disc was measured independently using a fiber-optic position sensor. Figure 4 (a) shows that there is good agreement between the ultrasonically measured displacement and that measured using the position sensor. The ultrasonically measured frequency also agrees well with the vibration frequency of the disc as indicated by the function generator setting.
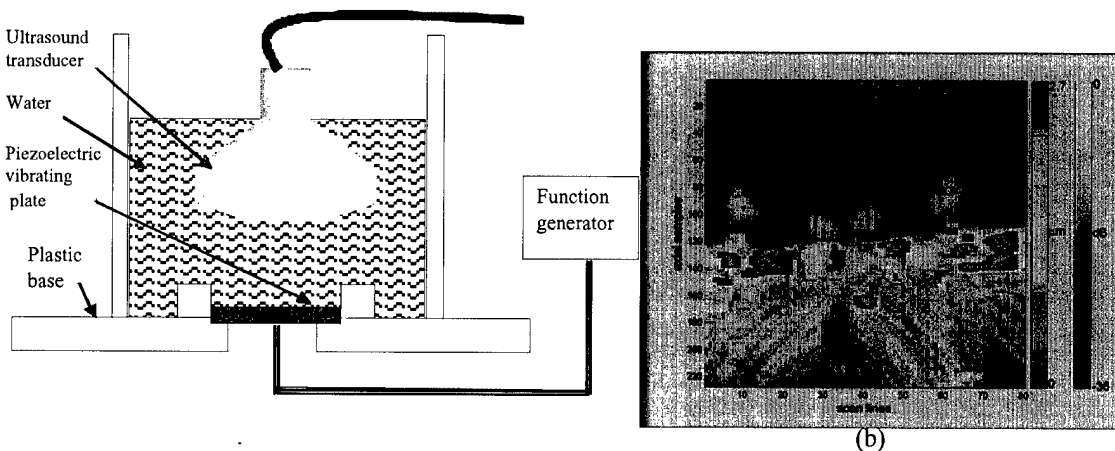

Figure 3 (a) Vibrating plate phantom (b) B-mode image of plate phantom overlaid with vibration amplitudes. The blue-orange colormap shows vibration amplitudes on a logarithmic scale. The maximum vibration amplitude is near the center of the plate and decreases towards the edges. The 256 depth samples correspond to 36 mm whereas the 90 lateral scan lines correspond to 51 mm.
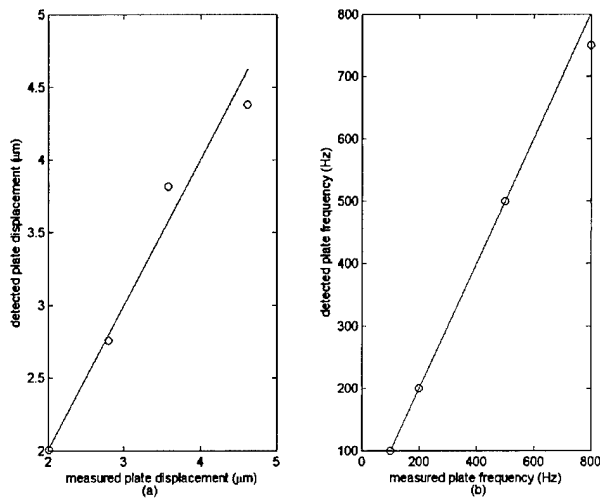
Figure 4. Detected vibration amplitudes (a) and frequencies (b) for vibrating plate phantom compared with the measured values.

To evaluate our algorithm *in vivo*, data were collected from a punctured artery and the lacerated liver and spleen of an anaesthetized pig, following a protocol approved by the University of Washington Institutional Animal Care and Use Committee. The femoral artery of the animal was punctured percutaneously with a Doppler-guided needle by a veterinary surgeon. To study organ bleeds, the liver and spleen were exposed and lacerated to cause bleeding. These organs were then imaged *in situ* through a block of tissue-mimicking gel as shown in Figure 5. A 5-Mhz linear probe was used for acquiring color-flow data @ PRF of 500 Hz with an ensemble length of 10.
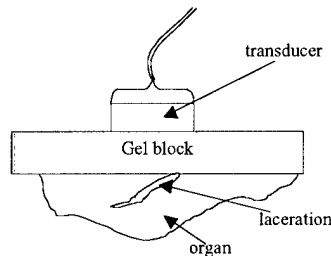

Figure 5. Imaging setup for organ bleeding. The lacerated organ is imaged *in situ* through a tissue-mimicking gel block.

Figure 6 (a) shows the color-Doppler image of the punctured femoral artery. The dotted box indicates the region of interest. The arrow indicates the approximate location of the puncture. Figure 6 (b) shows the vibration amplitude image with the vibrations are observed in the region of the puncture indicated by the arrow. Figure 7 (a) shows the B-mode image of the lacerated liver. The region marked "H" represents a hematoma at the bleeding site. Figure 7 (b) shows the vibration amplitude image with vibrations observed around the hematoma indicated by arrows. Figure 8 (a) shows the color-Doppler image of the lacerated spleen. The arrow marked "A" indicates the pooling blood from the laceration accumulated between the organ and the gel block. Some flow is observed at the bleeding site as indicated by the arrow marked "B". Figure 8 (b) shows the vibration amplitude image and vibrations are clearly observed at the bleeding site (indicated by the arrow).

These preliminary results indicate that vibrations are produced due to arterial bleeding at the bleeding site and it is possible to detect and create and image of these vibrations using our algorithm. Further studies are necessary to evaluate the effectiveness of localizing the bleeding

site based on these vibrations. Please see Publications (Section V) and the Appendix for publications and reprints related to this effort.
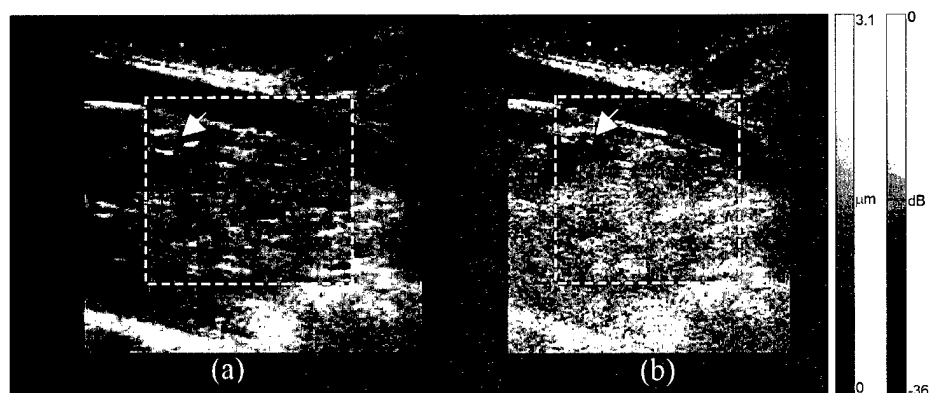

Figure 6. (a) color-Doppler and (b) vibration amplitude image of punctured femoral artery. The arrow indicates the bleeding site.
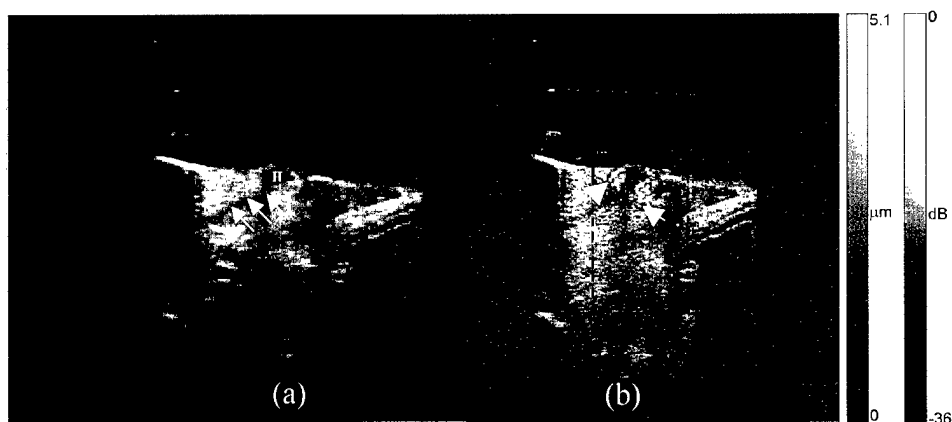

Figure 7. (a) B-mode image of lacerated liver. Arrows indicate the laceration and the hypoechoeic region marked "H" indicates a hematoma. (b) Vibration amplitude image. Vibrations indicated by arrows are observed around the hematoma at the bleeding site.
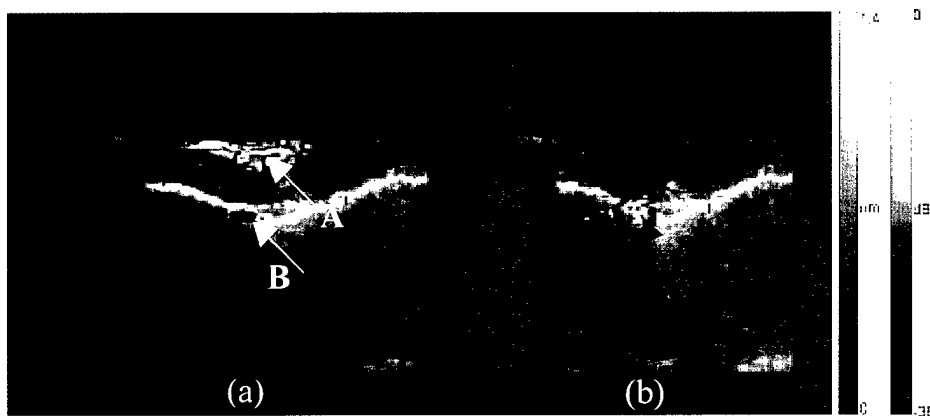

Figure 8. (a) color-Doppler image of lacerated spleen. Arrow marked "A" indicates pooled blood between the organ and gel block whereas "B" indicates the active bleeding site. (b) Vibration amplitude image with vibrations indicated by the arrow observed at the active bleeding site.

II.B. Therapy Delivery (Subtasks 2.1, 2.2)

II.B.1. Therapy Delivery: Real-Time Lesion Imaging Using RF Backscatter Monitoring Techniques

Widespread adoption of HIFU therapy for hemostasis or coagulative necrosis of tissue requires a complementary capability for targeting the treatment, monitoring progress of therapy, and post-treatment evaluation of therapeutic effectiveness. Current methods for bleeding detection using ultrasound (Doppler techniques) are typically only sensitive enough for bleeds that involve relatively high velocities. Many distributed injuries may result in large rates of blood loss through oozing capillary beds and widespread disrupted vasculature, and new techniques are being developed to detect and delineate such sites. Similarly, tissue characterization using medical ultrasound has very limited capability, and current modalities are lacking in resolution and specificity for tumor delineation and for HIFU lesion monitoring. It is well known that HIFU lesions are difficult to detect with diagnostic ultrasound *in vivo* and only relatively recently have new methods been developed to image hyperechoic regions closely correlated with the HIFU focal zone. The approach relies on the visualization of short-lived gas- or vapor-filled microbubbles, created by the combination of heat and large negative pressure in the focal zone, through interleaving of imaging frames and HIFU treatment. Though this method is useful for targeting, it is a qualitative measure of therapy and does not lead to an estimate of local temperature; furthermore, it is often associated with creation of a lesion and is not always suitable for aiming the therapy in sensitive areas.

We are continuing development of two techniques that lead to quantitative measures of changes in local tissue properties resulting from the application of HIFU therapy. The techniques both require access to the full ultrasound pressure waveforms, often called the "RF" signal, because the phase of the waveform contains a significant amount of information that is discarded in the creation of standard B-mode images. The two methods, one to observe changes in spectral content of the backscatter and the other to estimate local temperature change from the backsckatter, have been reported on previously. Here we provide a description of developments that have been limited (by available resources) to the temperature estimation problem.

This research has focused on the development of a model-based noninvasive temperature estimation algorithm for HIFU therapy monitoring in which the model parameters and $\Delta(T)$ are first non-invasively estimated in situ from travel time shifts directly measured from the ultrasound backscatter acquired during "probe" exposures. The model used to interpret and "fit" the data is the bioheat transfer equation, restricted to conductive heat transport (no advection). Estimates of $\Delta(T)$ from the probe experiments are then combined with local travel time changes measured during therapy and with constraints imposed by the bioheat equation to obtain quantitative temperature information.

The work completed within the grant performance period includes the development of an integrated experimental data acquisition system that can be used to acquire the raw ultrasound backscatter from a commercial ultrasound scanner during HIFU therapy (described previously). A signal processing based method to obtain estimates of local change in travel time shifts from ultrasound backscatter was developed and preliminary tests have been conducted; see Figure 9.

The temperature estimation method was validated against independent temperature measurements obtained using *in situ* thermocouples; see Figure 10. Of course, thermocouples are only needed to validate this completely noninvasive approach to map temperature using ultrasound. Future plans include *in vitro* validation with tissue, and a pilot study *in vivo*.

RF data are essential to obtain the sensitivity to the small changes in sound speed that are associated with HIFU induced temperatures: the sound speed changes less than 1% from 40 to 60 degrees C, and results in apparent motion on the order of microns over a distance of several centimeters! A significant complication in the inverse processing for local temperature using this measured change in travel time is due to the nonlinear (indeed it is multivalued) nature of the sound speed vs. temperature relationship. In future work, we will further validate the method, and explore feasibility in a pilot study *in vivo*. The heat transfer model will not be adequate if formation of bubbles occurs and changes the sound speed relationship, or if differential motion due to other factors such as mechanical shrinkage from denaturation (cooking) proves to be a significant contributor to observed tissue distortion.

Please see the Publications and Appendix for publications and reprints related to this research effort.
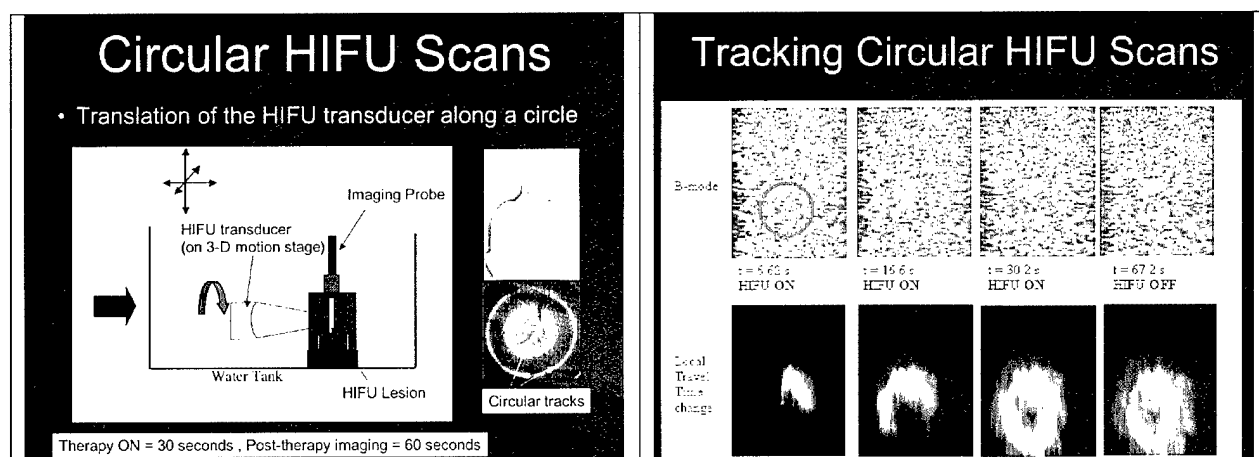

Figure 9. Travel Time Changes Elucidate Temperature Rise in a Phantom Material exposed to HIFU

(*Left*) Circular lesion tracks can be formed by exposing tissue to HIFU while moving the transducer in a circular pattern transverse to the beam direction. Such tracks may prove to be very efficient therapeutic protocols for HIFU. The imaging scanhead is placed transverse to the track to collect 2-D data for temperature mapping of the "painted lesion" therapy.

(*Right*) A circular scan was performed in a scattering and absorbing phantom material. Backscattered ultrasound signals can be used to track small changes in apparent position due to temperature related sound speed changes. The temperature dependence of the sound speed in the phantom is measured independently to provide the required mapping from travel time change to temperature rise. Several images obtained by processing the RF backscatter from a sequence of frames captured during the HIFU exposure illustrate the development and evolution of a thermal rise along the circular track. The start of the track is at "3 o'clock" and progresses counterclockwise for a full turn. The diffusion of heat is visible as a radial expansion of the red zone (coolest part) and a narrowing of the hottest zone (yellow).
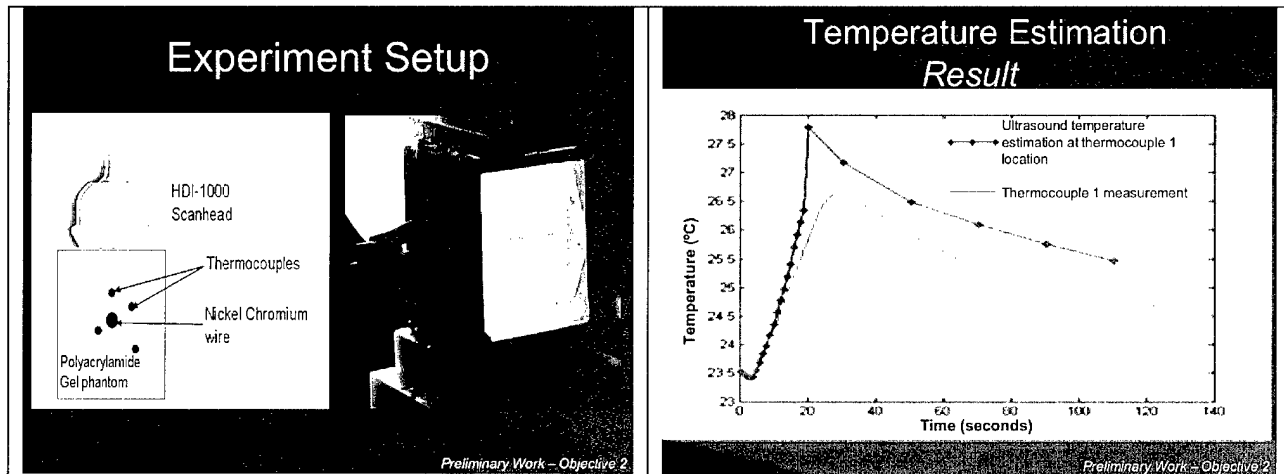
Figure 10. Validation experiment in gel phantom with a hot wire source
(*left*) A resistive wire is embedded in transparent gel along with 4 thermocouples. The phantom material has small scatterers embedded in it to provide backscatter; these are too small and too dilute to opacify the gel so the wire and thermocouples are clearly visible. An ultrasound scanhead is placed transverse to the wire to measure travel time changes resulting from temperature rise.
(*right*) One thermocouple record is plotted versus time in red (for the thermocouple closest to the wire). Temperature rise near the thermocouple location estimated from the ultrasound using the bioheat equation model-based algorithm is plotted versus time in blue. Values are obtained at the times corresponding to each frame acquisition. Agreement is very good, considering the small temperature rise of only 4 degrees at the peak, and the uncertainty in thermocouple position. This test indicates high sensitivity of the ultrasound method, and an accuracy of about 1 degree C. An accuracy of 5 degrees is expected to be adequate for HIFU therapy monitoring.

II.B.2 Therapy Delivery: Modeling

II.B.2.a KZK Bioacoustic Model Development and Validation

We completed a new KZK implementation of the acoustic wave equation that is coupled with the Bioheat Transfer Equation (BHTE); this was reported in the FY03 Annual Report. The new implementation allows us to simulate line and circular scanning protocols, make quantitative assessment of the effects of nonlinearity, and investigate treatment optimization to take potential advantage of nonlinear effects while minimizing unwanted thermal deposition. More detail can be found in the Proceedings articles provided in the Appendix.

II.B.2.b Wide-Angle Parabolic Equation Routine for 3-D Propagation

This grant supported an effort to develop a fast, wide-angle Parabolic Equation (PE) code to perform acoustic field modeling. The model was implemented using the split-step algorithm; the development generalizes the Kuttler s results to three dimensions. Theory and numerical results are presented below.

Consider the time-harmonic acoustic wave equation

$$\nabla^2 p + k^2 p = 0, \tag{2}$$

BEST AVAILABLE COPY

where, in general, both the pressure p and wavenumber k are functions of position $\mathbf{r} = (x, y, z)$. Consistent with the split-step method, we separate the effects of propagation from the effects of inhomogeneties in the medium; $k(\mathbf{r})$ is replaced by the constant reference wavenumber k_0 and the effects of the medium are included later. We assume the dominant propagation direction is in the z direction and rewrite (2)

$$\left[\frac{\partial^2}{\partial z^2} + \nabla_t^2 + k_0^2 \right] p = 0, \tag{3}$$

using the transverse Laplacian ∇_t^2. Factoring (3) yields

$$\left[\frac{\partial}{\partial z} + i\sqrt{k_0^2 + \nabla_t^2} \right] \left[\frac{\partial}{\partial z} - i\sqrt{k_0^2 + \nabla_t^2} \right] p = 0, \tag{4}$$

where we defer the discussion of how the square-root of an operator is interpreted. In the parabolic approximation, only outgoing waves are retained. Consistent with an $\exp(-i\omega t)$ time convention, we solve only

$$\frac{\partial p}{\partial z} = i\sqrt{k_0^2 + \nabla_t^2}\, p, \tag{5}$$

for propagation in $+z$. Equation (5) is the wide-angle parabolic equation. This partial differential equation is first-order in z and has solution

$$p(x, y, z) = \exp\left[iz\sqrt{k_0^2 + \nabla_t^2} \right] p(x, y, 0), \tag{6}$$

where the initial condition $p(x, y, 0)$ is the pressure on the $z = 0$ plane.

As noted by Kuttler [1999], the exponential of the square-root of an operator can be interpreted as a power series in the operator. To make this explicit,

$$\exp\left[iz\sqrt{k_0^2 + \nabla_t^2} \right] = 1 + \left[iz\sqrt{k_0^2 + \nabla_t^2} \right] + \tfrac{1}{2}\left[iz\sqrt{k_0^2 + \nabla_t^2} \right]^2 ..., \tag{7}$$

where

$$\sqrt{k_0^2 + \nabla_t^2} = k_0\sqrt{1 + \left(\nabla_t^2/k_0^2\right)} = k_0\left[1 + \tfrac{1}{2}\left(\nabla_t^2/k_0^2\right) - \tfrac{1}{8}\left(\nabla_t^2/k_0^2\right)^2 + ... \right]. \tag{8}$$

Combining (7) and (8) yields a power series in the transverse Laplacian $\nabla_t^2 = (\partial^2/\partial x^2 + \partial^2/\partial y^2)$.

We seek an implementation in the Fourier domain. First, define the two-dimensional forward Fourier transform,

$$\tilde{p}(k_x, k_y, z) = \int_{-\infty}^{\infty} \int_{-\infty}^{\infty} p(x, y, z) e^{-ik_x x} e^{-ik_y y}\, dx\, dy, \tag{9}$$

then substitute (6) through (8) into the integrand. It is well known that the Fourier transform of the derivative of a function is I times the Fourier variable times the transform of the function. Consequently, after transformation $\nabla_t^2 \rightarrow -(k_x^2 + k_y^2)$. Recombining the terms in the expansion yields

$$\tilde{p}(k_x, k_y, z) = \exp\left[iz\sqrt{k_0^2 - (k_x^2 + k_y^2)}\right]\tilde{p}(k_x, k_y, 0). \tag{10}$$

Taking the inverse transform associated with (9) gives the final wide-angle result for propagation through a homogeneous medium:

$$p(x, y, z) = \left(\tfrac{1}{2\pi}\right)^2 \int_{-\infty}^{\infty}\int_{-\infty}^{\infty} \exp\left[iz\sqrt{k_0^2 - (k_x^2 + k_y^2)}\right]\tilde{p}(k_x, k_y, 0)e^{+ik_x x}e^{+ik_y y}dxdy. \tag{11}$$

If the environment is inhomogeneous, (11) must be modified. As noted earlier, in the split-step algorithm, the effects of propagation and the effects of the range-dependent medium are separated. The field is first propagated as if through free-space using (11) and the medium is then included *a postori*. This is done by means of a phase screen. Let the phase screen be described by the transmittance function $T(x, y)$. Then the fields on the two sides of the phase screen are related by

$$p(x, y, z_+) = T(x, y)p(x, y, z_-). \tag{12}$$

The transmittance function accounts for the extra phase acquired by a ray traveling in the $+z$ direction, i.e.,

$$T(x, y) = \exp(i\phi(x, y)), \tag{12}$$

where over the range-step

$$\begin{aligned}\phi(x, y) &= \int_0^z [k(x, y, z') - k_0]dz' \\ &= k_0 \int_0^z n_f(x, y, z')dz'.\end{aligned} \tag{13}$$

The secondary form in (13) is in terms of the index of refraction perturbations n_f. Combining (11) and (12) gives the final wide-angle result:

$$p(x, y, z) = \left(\tfrac{1}{2\pi}\right)^2 T(x, y)\int_{-\infty}^{\infty}\int_{-\infty}^{\infty} \exp\left[iz\sqrt{k_0^2 - (k_x^2 + k_y^2)}\right]\tilde{p}(k_x, k_y, 0)e^{+ik_x x}e^{+ik_y y}dxdy. \tag{14}$$

There are multiple ways to derive the narrow-angle parabolic equation. One method starts by writing the pressure as e^{ik_0z} times a function that slowly varies in range. Substituting into (2) and ignoring higher derivatives, one arrives at a partial differential equation in z. This equation can then be solved by Fourier techniques. This derivation is straightforward and can be accomplished without expanding differential operators as was done above. The equivalent narrow-angle result can be derived directly from (13) by the approximation

$$\exp\left[iz\sqrt{k_0^2 - (k_x^2 + k_y^2)}\right] \approx e^{ik_0z} \exp\left[-i(k_x^2 + k_y^2)z/(2k_0)\right]. \tag{15}$$

Note that the narrow-angle result is equivalent to making the Fresnel approximation; see Goodman.

The split-step parabolic equation method was implemented in a Fortran 77 subroutine that makes use of the Numerical Recipes subroutine FOURN to calculate the necessary two-dimensional Fast-Fourier Transforms (FFTs). In typical usage, the main program calls the subroutine inside a do-loop that steps through the medium in range.

Four versions of the subroutine were implemented:

> Wide-angle PE: This version implemented the wide-angle parabolic equation developed in the theory section.

> Narrow-angle PE: This version implemented the traditional narrow-angle parabolic equation developed in the theory section.

> Spatially low-pass filtered propagation: The transverse sampling is often greater than half the wavelength. Consequently, the spatial frequencies considered when taking the FFT are less than the wavenumber. In medical applications, however, the transverse sampling might be less than a half-wavelength. Unless the field is low pass filtered, the evanescent waves will necessarily be included. Including the evanescent waves may, or may not be desirable; they might give a more accurate description of the propagating field, but they may also leave the calculation vulnerable to high spatial frequency noise. In this version of the subroutine, spatial frequencies greater than the wavenumber are set to zero. A narrow angle PE is used, but the wide angle PE could also be implemented.

> Frequency-domain (analytical) representation for the starting field: In the three versions listed above, the starting field for the routine is generated by simply sampling the acoustic field at the face of the transducer. In this version, the Fourier transform of the field at the initial range step is calculated analytically. Assuming cylindrical symmetry, the transform will typically be expressed in terms of a Bessel function. Before inverse transforming, the field might be low-pass filtered as well. The actual inverse transform is then performed using the same FFT routine as used to propagate the field. A narrow angle PE is used, but the wide angle PE could also be implemented as well.

As a test case, a scenario described by Wells [1977] was implemented: a plane disc transducer of radius 2.5 mm operating at 3 MHz. At this frequency, the radius of the disk was 5 wavelengths.

Numerical values:
        delxyz(1)= delxyz(2)=0.1e-3, delxyz(3)=0.2e-3 (as noted above, distances in meters).
        Mx=Ny=256, aK0=1.2566e+4 (consistent with 3 MHz and 1500 m/s).
The routine was called 250 times, meaning the field was advanced 5 cm.

Results for each of the four versions of the subroutine are first considered individually and then compared.

Wide-angle PE:
Figure 11 shows cross-sectional mapping of acoustic intensity for this routine. 250 range steps were taken, and the middle 101 of the 256 transverse points are shown. For range step equal to 0.2 mm, this corresponds to a total range of 5 cm. For transverse sampling of 0.1 mm, this corresponds to 1 cm, or twice the diameter of the transducer. The intensity is plotted in decibels, with 3 dB spacing between the colors. The total dynamic range is 30 dB.
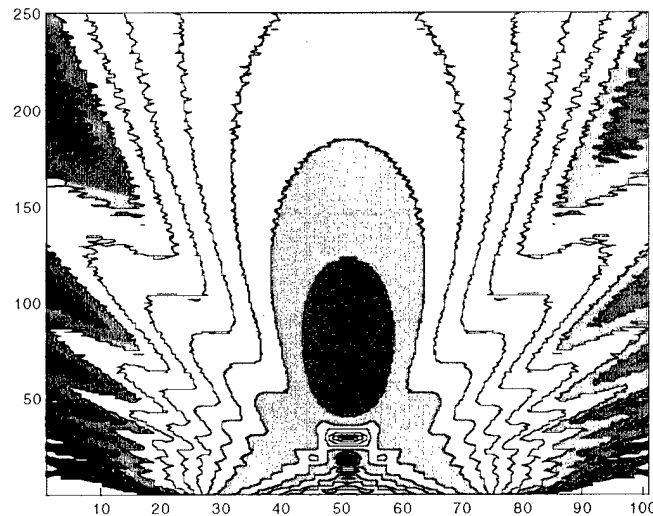

Figure 11: Wide-angle PE results

Narrow-angle PE:
Figure 12 shows cross-sectional mapping of acoustic intensity for this routine. Scaling and dimensions are the same as in Figure 11.

Figure 12: Narrow-angle PE results.

Spatially low-pass filtered propagation:
Figure 13 shows cross-sectional mapping of acoustic intensity for this routine. Scaling and dimensions are the same as in Figure 11.

Figure 13: Low-pass filtered, narrow-angle PE results.

Frequency-domain (analytical) representation for the starting field
Figure 14 shows cross-sectional mapping of acoustic intensity for this routine. Scaling and dimensions are the same as in Figure 11.
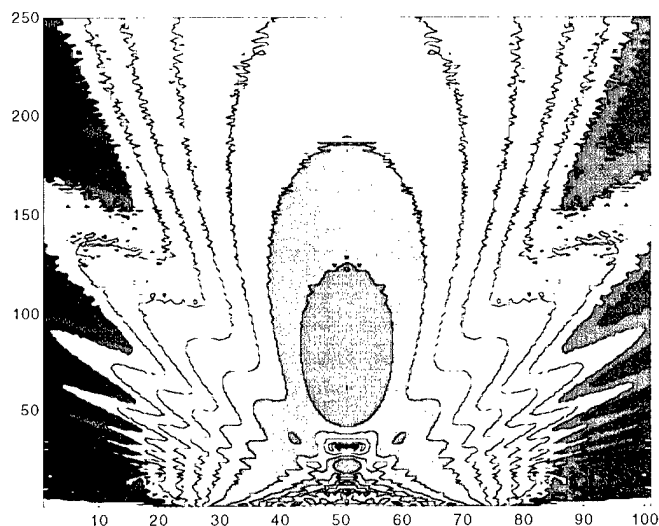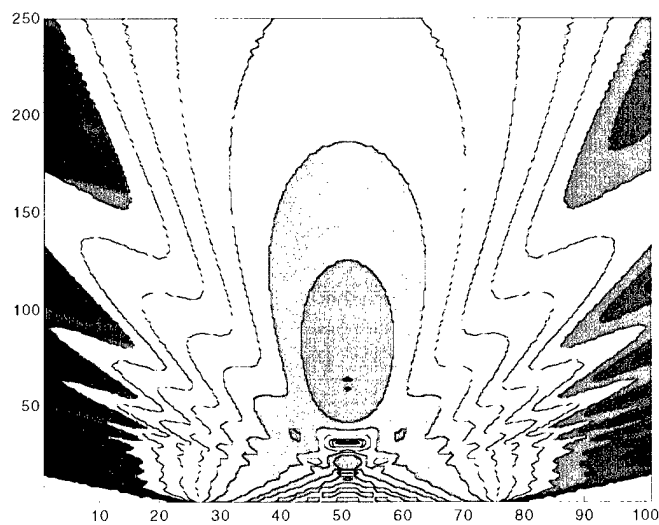
BEST AVAILABLE COPY

Figure 14: Analytical starting field, narrow-angle PE results.

In the near field, the acoustic intensity along the central axis exhibits a complicated pattern of peaks and nulls. Wells gives formulae for the location of these peaks and nulls. In Figure 15, the theoretical locations of these maxima and minima are tabulated and compared to the four versions of the parabolic equation that were implemented. The calculation is taken out to the Fresnel-Fraunhofer transition range.

All four PE routines peak near the transition range, as they should. Closer to the source, however, the different calculations go out of phase.

Figure 16 magnifies the results in the extreme near field. The locations of the peaks and null are incorrect for all three versions of the narrow angle PE. The wide angle version accurately locates the maxima and minima.

Figure 15: Intensity on axis.

Figure 16: Intensity on axis.

The wide-angle PE routine is clearly preferred in the near field as it correctly locates the peaks and nulls in the intensity. In the Fraunhofer (far-field) regi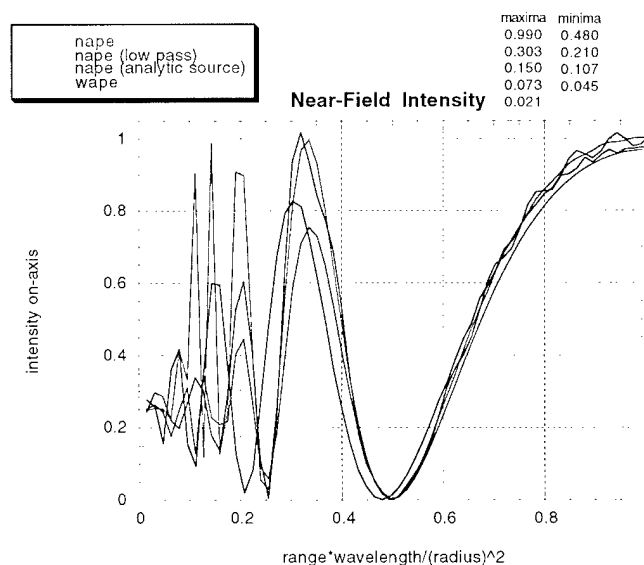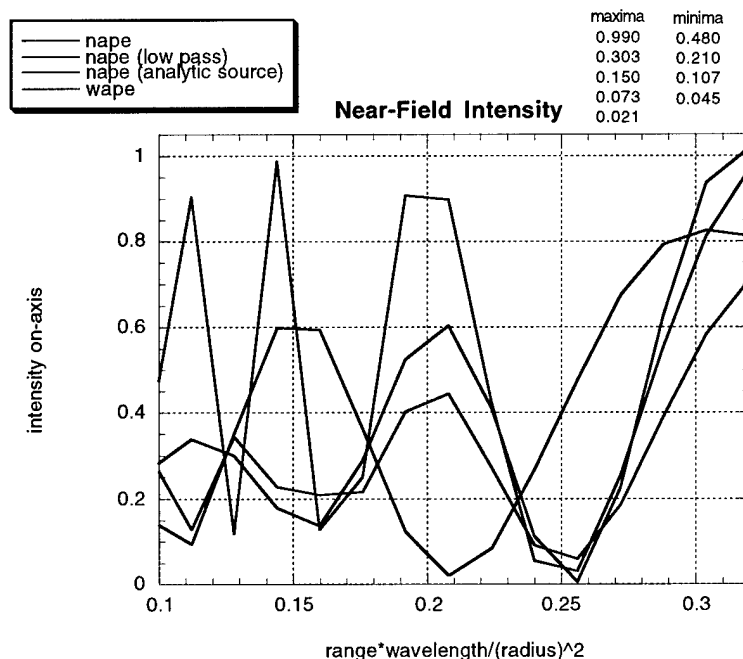me, the wide-angle solution shows some vulnerability to numerical noise; see Figure 10 beyond the 100th range step. Perhaps the ideal wide-angle routine would include the evanescent waves out to the Fresnel-Fraunhofer transition. At more distant ranges, the field should be low-pass filtered to smooth the beam pattern.

Section II.B.2.bReferences
J. W. Goodman, *Introduction to Fourier Optics* (Mc-Graw-Hill: San Francisco) 1968.

J. R. Kuttler, Differences between the narrow-angle and wide-angle propagators in the split-step Fourier solution of the parabolic wave equation, *IEEE Trans. Antennas Propagat.*, vol. 47, pp. 1131-1140, 1999.

P. N. T. Wells, *Biomedical Ultrasonics* (Academic Press: London) pp.26-31, 1977.

II.C   Systems Design and Development (Subtasks 3.2 and 3.31)

II.C.1 Systems Design & Development: Miniaturized Transducer Driving Electronics

An initial set of components for a portable, computer-controlled, phase-steered, image-guided HIFU system was developed and tested with support from this grant. This system uses a simple graphical software interface and a high speed USB 2.0 PC serial line to control multiple independent channels of high power transducer driving electronics. This therapy control display eventually will be fused with a diagnostic imaging display for image-guided operation (future

work under separate funding). The system's power amplifier design is based on mature class D power amplifier designs currently being used in other acoustic imaging systems. These amplifier designs were modified to handle the high-power requirements of a multi-channel HIFU system. The power amplifier electronics were modified to generate higher frequencies, increased power delivery capacity, increased efficiency, and thermal self-protection circuitry. Bench top testing of this design show it to have a power handling capacity over 60 W per channel (continuous). Similar to the power amplifier design work, signal generator electronics were developed based on existing designs currently being used in a multi-channel phased array transmitter system. This signal generator design provides up to 16 independent transmit signal channels having phase errors less than +/- 4 degrees at 2 MHz in a 3 square inch circuit card. The initial software prototype to interface these components and a standard PC was also completed.
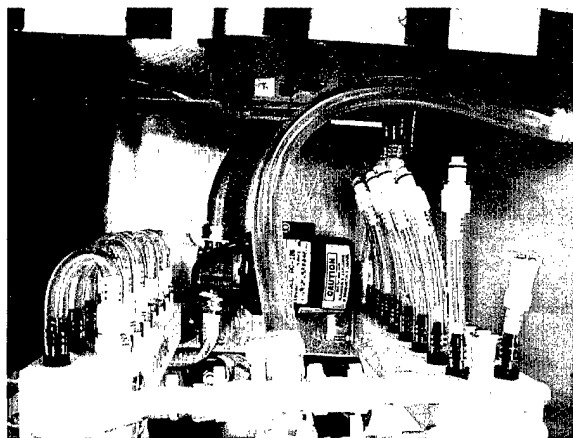
II.C.2 Systems Design & Development: Sonic Concepts Array and Electronics

CIMU has developed, through close collaboration with Sonic Concepts, Woodinville, Washington, a suite of HIFU transducers used in the exploration of coagulative therapy. Single element transducers, along with required electrical matching circuits (either external or integral to the transducer handle), have been manufactured and used *in vitro* and *in vivo* in a variety of experiments designed to develop therapeutic protocols to achieve hemostasis or coagulative necrosis. This experience had led to the development of annular arrays that would permit electronic control over the depth of the focal zone, and with central openings through which an imaging probe could be located. A coaxial arrangement has the advantage of ease of registration, and propagation of imaging and therapy beams through similar acoustic paths. This minimizes differences in aberration effects for the two modalities.

The first array was a 32-element array, operating at 2 MHz, with a 60 mm aperture, an 80 mm radius of curvature, and an opening sized for a P7-4 phased array imaging probe. Performance of the array was very good, as reported earlier. Unfortunately, before use in animal trials this array was damaged in testing at power primarily due to operator error. Nevertheless, several design weaknesses were raised and addressed in the follow-up design. These include: reducing the number of rings to improve manufacturability and transducer efficiency at the expense of focusing range, filling the back after wire-bond with a low loss lightweight material design to completely seal the interior region from potential water leaks, and simplifying the shape of the central opening by making it circular. The design results in a transducer that is less expensive to make, about 50% more efficient (from about 50% to about 75% efficiency), and much more robust electrically and mechanically. The unit has been manufactured and delivered by Sonic Concepts, and as of the close of this grant, was ready for testing and integration into a new housing. The housing is being designed under separate funding. The geometric shape of the spherical element from which the 5-element transducer is machine is identical to the 32-element unit: 60 mm aperture and 80 mm radius of curvature. To accommodate close focusing, future work (under separate funding) includes low-loss lens design and development. Figure 17 illustrates the transducer design and the completed unit.

(a) Schematic illustrating the rear view of the array.

(b) Diagram showing the 5 elements, and the relative hole sizes. The hole was made to accommodate the 20 mm TV probe.

(c) Connector side – oblique view.

(d) Front face – oblique view.

Figure 17. Sonic Concepts phased array.

We reported earlier (FY 03 Annual Report) on the design and manufacture of a 32-channel signal generation and power amplifier system, with software control and a simple clinical interface. The initial system was completed during the grant performance period, and was used to drive the 32-channel array, and also an 11-element array manufactured by Imasonic, France. During the course of testing the Imasonic array, the array failed due to unknown causes. Several hypotheses are under consideration, but it appears likely that the amplifiers drove the array in an unwanted manner (wrong frequency and power) and without the operator becoming aware of the problem. Because of the uncertainty, we investigated the stability of the amplifiers and explored ways of ensuring adequate and uniform cooling of the active elements (power transistors) that dissipate substantial heat and can fail at high temperatures.

The size of the multi-channel rack, combined with the need for reliable and uniform cooling requires individual cooling ducts for each amplifier. This is most easily achieved by water-cooling of the active elements. Figure 18 illustrates the brass tubing ducts mounted on the heat sinks and front faces of the power transistors. These are connected to a water distribution manifold that distributes and collects flow from 16 boards. (We reduced the channel count to

meet current transducer designs.) The system maintains a transistor case temperature of less than 60 °C, which is well within specifications.
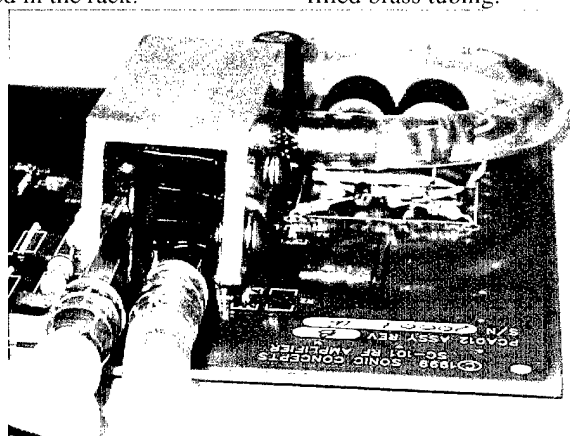
Future work under separate funding includes further redesign of the power amplifier electronics to improve stability and reliability, following by *ex vivo* and *in vivo* demonstration of the entired system (phased array, electronics, and image-guidance and control interface.

(a) Top view of the water coolant distribution manifold. The water circulation pump is visible at the back of the picture (bottom of the rack). A few circuit boards (one per channel) are visible mounted in the rack.

(b) Oblique view of a single channel circuit board, with water-cooling modifications. The power transistors are cooled both front and back by direct contact with water-filled brass tubing.
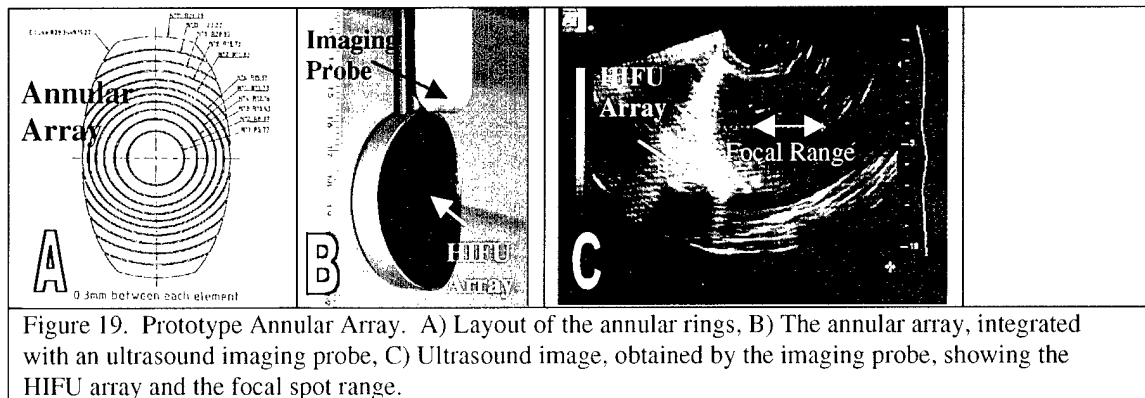

(c) The brass tubing is held in place with custom clamps made from aluminum U-channel extrusion. The original heat sinks were left in place for mechanical stability.

Figure 18. Driving Electronics for Phased Array

II.C.3 Systems Design & Development: Imasonic Array

We have developed an annular array with the following specifications:

> Focal Depth Adjustment 3-6 cm;
> Transducer Material: Piezocomposite;
> Center Frequency: 3 MHz;
> 11 Elements: 6 complete annuli, 5 truncated annuli; All Equal Area;
> Maximum Focal Intensity: 3000 W/cm^2 (see Fig. 19).

Figure 19. Prototype Annular Array. A) Layout of the annular rings, B) The annular array, integrated with an ultrasound imaging probe, C) Ultrasound image, obtained by the imaging probe, showing the HIFU array and the focal spot range.

An 11-element (concentric rings) array using 1-3 piezocomposite technology was designed and manufactured at Imasonic Corporation. The design included 6 complete rings in the center, and 5 side-truncated rings in the periphery. The natural radius of curvature of all elements is 50 mm. The HIFU transducer has about 1 MHz bandwidth for all 11 elements. The impedance of all elements is approximately 50 ohms, with better than 10% accuracy for both real and imaginary parts, using a custom-made matching network. The adjacent element cross coupling is less than -40 dB. High power measurements on the central transducer element showed more than 75% efficiency, at surface intensity of 2.66 W/cm^2. Schlieren imaging showed effective focusing at all focal lengths (30-60 mm).

We purchased a commercial electronic driving system (Advanced Surgical Systems, Inc., Arizona) to power the Imasonic array. The control software interface will be developed under separate funding, and will be implemented using Labview and C language. The 32-channel unit is composed of two 16 channel sub-systems. One sub-system operates at a frequency range of 1.5-2.5 MHz; the second operates from 2.5-3.5 MHz. The subsystems enable expanded treatment capacity, with the lower frequencies (1.5-2.5 MHz) offering increased treatment depth. The system is capable of providing a maximum of 60W per individual channel, with maximum overall power of 800 W, at each time point. This maximum power limit translates into 50 W per individual channel when all channels are operating. The software control system being developed under separate funding will monitor power characteristics to ensure safe operation. The demonstration system of array, driving electronics and software control system will be tested *in vivo* under separate funding.

II.D   Animal Testing of Systems (Subtask 4.1)

II.D.1 Animal Testing of Systems: Vibrometry for Bleeding Detection

Initial *in vitro* phantom and *in vivo* animal testing of vibromety bleeding detection algorithms was discussed in section II.A.1 above.

II.D.2 Animal Testing of Systems: Optimal Parameters of Hemostasis

In vivo animal testing to investigate optimal parameters of acoustic hemostasis was reported in some detail in the FY 03 Annual Report. This effort continued until the end of the performance

period. A significant finding is that the HIFU-made blood/tissue homogenate, or "coagulum," acts as an effective hemostatic seal over the injury site (see Figure 20). A study was conducted to document the advantage or disadvantage of producing the homogenate. In treatments with homogenate formation, hemostasis was achieved in 76±1.3 seconds (Mean ± Standard Error Mean: SEM) at 80 W. In treatments without homogenate formation (at 80 W), hemostasis was achieved in 106±1.3 seconds). At 100 W, hemostasis was achieved in 46±0.3 seconds. The time required for homogenate formation, at 80 and 100 W were 60±2.5 seconds and 23±0.3, respectively. The homogenate temperature was 82 °C (SEM 0.6 °C), and the non-homogenate tissue temperature at the treatment site was 60 °C (SEM 0.4 °C). The smear and histological analysis (see Figure 21) showed significant blood components and cellular debris in the homogenate, with some intact cells. The HIFU-induced homogenate of blood and tissue resulted in a statistically significant shorter HIFU application time for hemostasis. The incisions with homogenate had higher temperatures as compared to incisions without homogenate. Further studies of the correlation between homogenate formation and temperature must be done, as well as studies on the long-term effects of homogenate in achieving hemostasis.

Figure 20. The coagulum being formed in liver near the tip of the applicator (left image) and magnified view of the emulsion with bubbles present (right image).
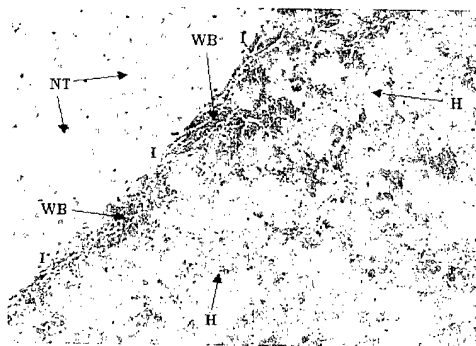

Figure 21. Sample of intact in situ necrotic tissue (NT) from site of incision (I) treated with HIFU. Tissue homogenate (H) is seen with mass of destroyed, undifferentiable cells. Some whole blood cells (WB) are seen at the edge of incision.

II.D.3 Animal Testing of Systems: Array System Testing

Technical difficulties with the arrays and driving electronics prevented performing *in vivo* testing during the performance period of the grant. These tests will be conducted under separate funding in 2004. The Imasonic array underwent preliminary bench and *in vitro* testing before the grant closed. Bench-based beamforming and electrical tests were completed; this work was discussed in the FY 03 Annual Report. Testing *in vitro* with a tissue-mimicking phantom verified the formation of a hyperechoic region at the focus (see Figure 22).
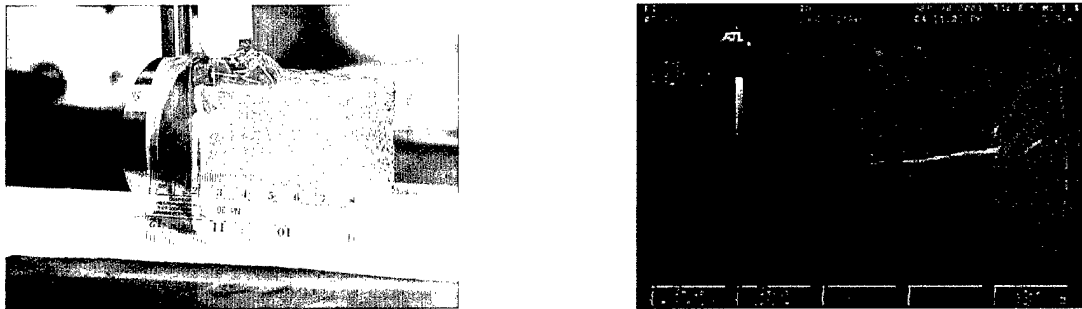
Figure 22. (a) Imasonic array lesion formation in a tissue mimicking phantom. (b) Ultrasound image showing hyperechoic region in focus.

III. DEGREES AND FELLOWSHIPS

The following individuals earned degrees through funding provided in part by this project:

- George Barrett, March 2003, dissertation title, "Kinesiographic lesion monitoring (KLM)."
- Tyrone Porter, July 2003, dissertation title, "An investigation of the synergy between ultrasound and membrane-disruptive polymers and its effect on cell membranes."

The following students are continuing research efforts that were initiated under this project:

- Ajay Anand, Electrical Engineering Ph.D. candidate, dissertation title "A Model-Based Noninvasive Temperature Estimation Technique for HIFU Therapy Monitoring Using Backscattered Ultrasound."
- Siddhartha Sikdar, Electrical Engineering Ph.D. candidate, tentative dissertation title "Ultrasonic Techniques for Imaging Pathological Tissue Vibrations"
- Jessica Foley, Bioengineering Ph.D. student.

IV. INTELLECTUAL PROPERTY

The following invention disclosures were filed under this grant:

OTL Ref#2031-3997
Inventor(s): Shahram Vaezy
Title of Invention: Transvaginal, Ultrasound Image-Guided,
Hysterescopic HIFU Device for Treatment of Uterus and Pelvis Date
Received: 8/4/2003

OTL Ref#2031-4025
Inventor(s): Kirk W. Beach, Yongmin Kim, Siddhartha Sikdar Title of
Invention: Transcutaneous Localization of Internal Bleeding by
Two-dimensional Ultrasonic Imaging of Tissue Vibrations Date Received:

10/3/2003 Provisional Patent 60/508,554 File Date: 10/3/2003

OTL Ref#2031-4070
Inventor(s): Ajay Anand, Peter J. Kaczkowski
Title of Invention: Model-Based Noninvasive Temperature Monitoring for
HIFU Therapy Using Backscattered Ultrasound Date Received: 11/20/2003

OTL Ref#3078-4076
Inventor(s): R. Lee Thompson, Jason Seawall, Scott Bachelor Title of
Invention: Background IP Information for Low-cost Imaging Sonar System
with Increased Field of View Date Received: 12/4/2003

Form DD 882, Report of Inventions and Disclosures, will be forward separately from the UW
Office of Technology Licensing.

V.   PUBLICATIONS (full or partial funding by this project)

Refereed Papers

Anand AJ, Kaczkowski PJ, Daigle RE, Huang L, Paun M, Beach KW, and Crum LA, "Using the
ATL HDI-1000 ultrasound scanner to collect demodulated RF data for monitoring HIFU lesion
formation," *Proc SPIE*, **5035**, 316-326 (2003).

Anand AJ, Kaczkowski PJ, "Monitoring formation of High Intensity Focused Ultrasound (HIFU)
induced lesions using backscattered ultrasound", *Acoustic Research Letters Online*, July 2004,
Volume 5, Issue 3, p. 88-94. (paper can be found at
http://scitation.aip.org/getabs/servlet/GetabsServlet?prog=normal&id=ARLOFJ00000500000300
0088000001&idtype=cvips&gifs=Yes)

Cornejo C, Vaezy S, Jurkovich J, Paun M, Noble M, Starr F, Sharar S, Martin RW, "High
Intensity Ultrasound Treatment of Blunt Abdominal Solid Organ Injury: An Animal Model,"
submitted to J. Trauma.

Hwang JH, Kimmey M, Martin R, Vaezy S, "Acoustic hemostasis of lacerated veins: Potential
applications for gastrointestinal bleeding," Gastrointestinal Endoscopy, **55** (5): M1883 Suppl. S
(2002).

Noble ML, Vaezy S, Keshavarzi A, Paun M, Prokop AF, Chi EY, Cornejo C, Sharar SR,
Jurkovich GJ, Martin RW, Crum LA, "Spleen hemostasis using high-intensity ultrasound:
survival and healing," *J. Trauma*, **53** (6), 1115-1120 (2002).

Prokop AF, Vaezy S, Noble ML, Kaczkowski PJ, Martin RW, Crum LA. Polyacrylamide Gel as
an Acoustic Coupling Medium for Focused Ultrasound Therapy. Ultrasound Med Biol., 29 (9),
1351-1358 (2003).

Sikdar S, Vaezy S, Beach B, and Kim Y (2003) Transcutaneous Localization of Arterial Bleeding by Two-dimensional Ultrasonic Imaging of Tissue Vibrations, Proceedings of the IEEE Ultrasonics Symposium, Hawaii, pp. 1820-1823.

S. Sikdar, S. Vaezy, K. W. Beach and Y. Kim, Ultrasonic Technique for Imaging Tissue Vibrations, Ultrasound Med. Biol., submitted, 2003.

Vaezy S, Noble M, Keshavarzi A, Paun M, Prokop A, Cornejo C, Sharar S, Chi EY, Crum LA, and Martin RW, "Liver hemostasis using high intensity ultrasound: repair and healing," J. Ultrasound Med., 23 (2), 217-25 (2004).

Vaezy S, Vaezy S, Starr F, Chi E, Cornejo C, Crum LA and Martin RW. Optimal Parameters for Intra-operative Acoustic Hemostasis. European Journal of Ultrasound, 2003, Submitted.

S. Vaezy, B. Huguenin, G. Fleury, J. Flexman, and R. Held, "A Transvaginal Image-Guided High Intensity Ultrasound Array," IEEE Ultrasonics Symposium Proceedings, CD7 (2003).

S. Vaezy, S. Vaezy, F. Starr, E. Chi, C. Cornejo, L. Crum, and R. Martin, (2004) Intra-Operative Acoustic Hemostasis of Liver: Production of a Homogenate for Effective Treatment, *Ultrasonics*, Submitted.

Zderic V, Andrew M, Martin R, Pezzotti N, and Vaezy S, "Attenuation of Porcine Tissues In Vivo After High Intensity Ultrasound Treatment," Ultrasound Med Biol., 30 (1), 61-66 (2004).

Books, Book Chapters and Proceedings

Anand A, Huang L, Kaczkowski P, Daigle R, Crum L, "Using ATL HDI-1000 Ultrasound Scanner for Tissue Elasticity Imaging," Proceedings of the First International Conference on the Ultrasonic Measurement and Imaging of Tissue Elasticity, Niagara Falls, Ontario, Canada (Oct. 2002).

Andrew MA, Kargl SG, Kaczkowski PJ, Cunitz BW and Brayman AA. Circular Scanned Thermal Lesions in Ex Vivo Bovine Liver. Proceedings of the 3rd International Symposium on Therapeutic Ultrasound, Lyon, France, 23 – 25 June 2003, in press.

Andrew MA, Crum LA, and Vaezy S (editors), Proceedings of the 2nd International Symposium on Therapeutic Ultrasound, University of Washington, Seattle, Washington, 2003.

Crum LA, Bailey M, Carter S, Curra F, Kaczkowski P, Kargl S, Image-guided acoustic hemostasis, in New Acoustics: Selected Topics, C. Ranz-Guerra and J. A. Gallego-Juarez, eds., (Consejo Superior de Investigaciones Cientificas, Madrid), pp 26-36 (2002).

Hwang JH, Brayman A, Vaezy S. Pulsed High-intensity Focused Ultrasound Inducing Endothelial Cell Injury in Vessels Infused with Ultrasound Contrast Agent. Proceedings of the 2nd International Symposium on Therapeutic Ultrasound. 29 July-2 August 2002. Seattle, WA.

Kaczkowski PJ, Keilman GW, Cunitz BW, Martin RW, Vaezy S, and Crum LA, "High Intensity Focused Ultrasound (HIFU) array system for Image-guided ablative therapy (IGAT)," *SPIE Photonics West*, BIOS 2003, in session 4954 (2003).

Kaczkowski PJ and Anand A. RF Ultrasound Backscatter Processing for Guidance and Monitoring of HIFU Therapy. Proceedings of the 3rd International Symposium on Therapeutic Ultrasound, Lyon, France, 23 – 25 June 2003, in press.

Martin RW, Vaezy S and Chi E. Investigation of HIFU Produced Emulsion for Acoustic Hemostasis. Proceedings of the 3rd International Symposium on Therapeutic Ultrasound, Lyon, France, 23 – 25 June 2003, in press.

Noble ML, Vaezy S, Crum LA. Investigation of the Opacification of High Intensity Ultrasound-Induced Thermal Lesions in a Tissue-Mimicking Phantom. Proceedings of the 2nd International Symposium on Therapeutic Ultrasound. 29 July-2 August 2002. Seattle, WA.

Prokop AF, Vaezy S, Noble ML, Martin RW. Polyacrylamide Gel as an Acoustic Coupling Medium for Focused Ultrasound Therapy. Proceedings of the 2nd International Symposium on Therapeutic Ultrasound. 29 July-2 August 2002. Seattle, WA.

Rouseff D. A Wide-Angle Parabolic Equation Routine for 3-D Propagation, CIMU Internal Report, 2003.

Abstracts /Presentations

Anand A, Huang L, Kaczkowski P, Daigle R, Crum L. Using ATL HDI-1000 Ultrasound Scanner for Tissue Elasticity Imaging. Presented at: First International Conference on the Ultrasonic Measurement and Imaging of Tissue Elasticity, Niagara Falls, Ontario, Canada, October 2002.

Anand AJ, Kaczkowski PJ, "Ultrasound RF-signal analysis of HIFU-induced lesions", Abstracts of 28th Ultrasonic Imaging and Tissue Characterization Symposium, Arlington, VA, published in Ultrasonic Imaging, Vol. 25 (1), January, 2003.

Anand AJ, Kaczkowski PJ, "Monitoring evolution of HIFU-induced lesions with backscattered ultrasound", 145th Meeting of the Acoustical Society of America, Nashville, TN, 28 April – 2 May, 2003, J. Acoust. Soc. Am., Vol. 113, No. 4, Pt. 2, p 2310 (2003).

Andrew MA, Kaczkowski PJ, Cunitz BW, Brayman AA and Kargl SG. Study of a scanning HIFU therapy protocol, Part II: Experiment and results. Presented at: 145th meeting of the Acoustical Society of America, Nashville, Tennessee, 28 April – 2 May, 2003.

Andrew MA, Kargl SG, Kaczkowski PJ, Cunitz BW and Brayman AA. Circular Scanned Thermal Lesions in Ex Vivo Bovine Liver. Presented at: 3rd International Symposium on Therapeutic Ultrasound, Lyon, France, 23 – 25 June 2003.

Crum LA, Andrew MA, Bailey M, Beach KW, Brayman AA, Curra FP, Kaczkowski PJ, Kargl SG, Martin R, and Vaezy S. Acoustic Hemostasis. Presented at: 145th meeting of the Acoustical Society of America, Nashville, Tennessee, 28 April – 2 May, 2003.

Cunitz B, and Kaczkowski P. Mapping high power ultrasonic fields using a scanned scatterer. Presented at: 143rd meeting of the Acoustical Society of America Jun 3-7th 2002.

Curra FP, Kargl SG, and Crum LA, "3-D Full Wave Ultrasonic Field and Temperature Simulations in Inhomogeneous Biological Tissue," Proceedings of the 16th International Symposium on Nonlinear Acoustics 2002, Moscow, Russia, 19-23.

Hwang JH, Brayman A, Vaezy S. Pulsed High-intensity Focused Ultrasound Inducing Endothelial Cell Injury in Vessels Infused with Ultrasound Contrast Agent. Presented at: 2nd International Symposium on Therapeutic Ultrasound. 29 July-2 August 2002. Seattle, WA.

Kaczkowski PJ, Keilman GW, Cunitz BW, Martin RW, Vaezy S, and Crum LA. High Intensity Focused Ultrasound (HIFU) array system for Image-guided ablative therapy (IGAT). Presented at: SPIE Photonics West, BIOS 2003.

Kaczkowski PJ and Anand A. RF Ultrasound Backscatter Processing for Guidance and Monitoring of HIFU Therapy. Presented at: 3rd International Symposium on Therapeutic Ultrasound, Lyon, France, 23 – 25 June 2003.

Martin RW, Vaezy S and Chi E. Investigation of HIFU Produced Emulsion for Acoustic Hemostasis. Presented at: 3rd International Symposium on Therapeutic Ultrasound, Lyon, France, 23 – 25 June 2003.

Noble ML, Vaezy S, Crum LA. Investigation of the Opacification of High Intensity Ultrasound-Induced Thermal Lesions in a Tissue-Mimicking Phantom. Presented at: 2nd International Symposium on Therapeutic Ultrasound. 29 July-2 August 2002. Seattle, WA.

Prokop AF, Vaezy S, Noble ML, Martin RW. Polyacrylamide Gel as an Acoustic Coupling Medium for Focused Ultrasound Therapy. Presented at: 2nd International Symposium on Therapeutic Ultrasound. 29 July-2 August 2002. Seattle, WA.

Vaezy S. Acoustic Hemostasis: MRI-Guided Focused Ultrasound Surgery. Presented at: Workshop on MRI-Guided: Focused Ultrasound Surgery. 19-21 June 2002. Cambridge, MA.

Vaezy S, Martin RW, Nicolaou S, Cornejo C, Jurkovich G, Sharar S, Crum LA. High Intensity Focused Ultrasound for Treatment of Bleeding and Air Leaks due to Lung Trauma. Presented at: 1st Pan-American/Iberian Meeting on Acoustics/Acoustical Society of America Meeting. 2-6 December 2002. Cancun, Mexico.

Vaezy S, Wyzgala M, Keilman G. A Needle-size Hydrophone and Thermocouple for High-Intensity Focused Ultrasound. Presented at: 1st Pan-American/Iberian Meeting on Acoustics/Acoustical Society of America Meeting. 2-6 December 2002. Cancun, Mexico.

Vaezy S, Vaezy S, Starr F, Chi E, Cornejo C, Sharar S, Crum L, and Martin R. Optimal Parameters of High Intensity Ultrasound for Intraoperative Hemostasis, (2003) Presented at: World Federation for Ultrasound in Medicine and Biology and American Institute of Ultrasound in Medicine, Montreal, Canada, Ultrasound in Medicine and Biology, Vol. 29(5S):S212.

Vaezy S, Vaezy S, Starr F, Chi E, Cornejo C, Crum L, and Martin R. Optimal Parameters for Intra-Operative Acoustic Hemostasis, (2003) Presented at: Ultrasonics International, Granada, Spain, 3.35B.